Quaternary Science Reviews 29 (2010) 3327–3335

Contents lists available at ScienceDirect

Quaternary Science Reviews

journal homepage: www.elsevier.com/locate/quascirev

East Asian monsoon evolution and reconciliation of climate records from Japan and Greenland during the last deglaciation

Chuan-Chou Shen [a,*], Akihiro Kano [b], Masako Hori [c,1], Ke Lin [a], Tzu-Chien Chiu [d], George S. Burr [e]

[a] High-precision Mass Spectrometry and Environment Change Laboratory (HISPEC), Department of Geosciences, National Taiwan University, Taipei 106, Taiwan ROC
[b] Division of Evolution of Earth Environment, Graduate School of Social and Cultural Studies, Kyushu University, 744 Motooka, Fukuoka, 819-0395, Japan
[c] Department of Earth and Planetary Systems Science, Hiroshima University, Kagamiyama 1-3-1, Higashi-Hiroshima, 739-8526, Japan
[d] Institute of Earth Sciences, Academia Sinica, P.O. Box 1-55, Nankang, Taipei 115, Taiwan ROC
[e] Department of Physics, University of Arizona, Tucson, Arizona 85721, USA

ARTICLE INFO

Article history:
Received 26 February 2010
Received in revised form
4 August 2010
Accepted 16 August 2010

ABSTRACT

East Asian monsoon (EAM) evolution during the last deglaciation has been shown repeatedly to be aligned with paleoclimatic changes in the North Atlantic, based on climate reconstructions comparing Asian speleothem records with Greenland ice cores. In contrast to this finding, paleoclimatic reconstructions based on Lake Suigetsu sediment cores suggest that past EAM variability in Japan was not always coherent with climatic variability recorded in Greenland ice cores. We resolve this discrepancy using an absolute-dated stalagmite $\delta^{18}O$ record that covers the period between 15.5 and 10.7 thousand years before present (ka, before AD 1950). This stalagmite record is from nearby Maboroshi cave, Japan, and shows climate changes that are synchronous with those of Chinese caves and Greenland ice cores. Our results support an effective teleconnection between low- and high-latitudinal climate systems during the transitions into the Bølling–Allerød (BA) warming at 14.6 ka and the Younger Dryas cooling at 12.8 ka in the North Atlantic. However, our results also indicate monsoonal intensification during the BA, coincident with decreasing temperatures in Greenland from 14.6 to 12.8 ka. We explain this decoupling as a result of the interhemispheric bipolar seesaw climate system. Discrepancies between Lake Suigetsu radiocarbon age data sets and other radiocarbon calibration archives can also be removed when our Maboroshi record is used to adjust the Lake Suigetsu age model, as well as resolving temporal ambiguities in the Lake Suigetsu paleoclimate record.

1. Introduction

Structures and mechanisms of the paleo-East Asian monsoon (EAM) have been explored since the beginning of the 1990s (e.g., Clemens et al., 1991; Prell and Kutzbach, 1992; Sirocko et al., 1996; Heusser and Morley, 1997; Huang et al., 1997; Morley and Heusser, 1997; Wang et al., 1999; An, 2000). The exact timing of EAM variability in the late Pleistocene was first revealed by absolute-dated stalagmite $\delta^{18}O$ records from Hulu cave, China (Wang et al., 2001). More details of EAM histories in different time windows in the Pleistocene were subsequently established over the past decade (Yuan et al., 2004; Wang et al., 2005, 2008; Cheng et al., 2006; Cai et al., 2006; Zhang et al., 2008; Cheng et al., 2009; Yang et al., 2010). The archive records of EAM are characterized by orbitally-controlled cycles, overlain by millennial events, synchronous with Greenland temperature variations (e.g., Wang et al., 2001; Cheng et al., 2006).

During the last deglaciation, consistency in the timing and duration of the Bølling–Allerød (BA) and Younger Dryas (YD) periods observed in Chinese speleothem records and Greenland ice-core records provide evidence for a teleconnection between the EAM system and North Atlantic climate (e.g., Wang et al., 2001, 2005; Yang et al., 2010). The overall EAM dynamics at Terminations I–IV have been discussed by Cheng et al. (2009). However, the influences of high-latitudinal forcings and meridional energy transport mechanisms are still not fully understood, particularly those with regard to possible regional differences within the EAM. One example is the reconstructed climate record from Lake Suigetsu, Japan, which features marked asynchroneities when compared to Greenland during the last deglaciation (Nakagawa et al., 2003, 2006), especially at the transitions into the BA (t-BA) at 14.6 thousand years before present (ka, before AD 1950) and YD (t-YD) at 12.8 ka in the Greenland records (Steffensen et al., 2008).

* Corresponding author. Tel.: +886 2 3366 5878; fax: +886 2 3365 1917.
[1] Present address: Earth Dynamic System Research Center, National Cheng Kung University, No.1 University Road, Tainan City 701, Taiwan ROC.
E-mail address: river@ntu.edu.tw (C.-C. Shen).

0277-3791/$ – see front matter © 2010 Elsevier Ltd. All rights reserved.
doi:10.1016/j.quascirev.2010.08.012

These asynchroneities could reflect regional climatic differences between Lake Suigetsu and Chinese caves (e.g., Wang et al., 2001; Yang et al., 2010) within the EAM. This is possible since Lake Suigetsu lies along the northeast margin of the EAM region and the Chinese caves (Wang et al., 2001; Yang et al., 2010) is located far to the south and west on the Asian continent (Fig. 1). To test this possibility we have produced a decadally-resolved stalagmite $\delta^{18}O$ record of climate change during 15.5–10.7 ka using samples from Maboroshi Cave, Japan, near Lake Suigetsu. We interpret this record in terms of variations in forcings and pathways of the EAM at different climate intervals. Our results place stringent temporal constraints on the Lake Suigetsu paleoclimate record and show that the paleoclimate patterns at Lake Suigetsu are actually synchronous with Chinese cave speleothem records and with those in Greenland.

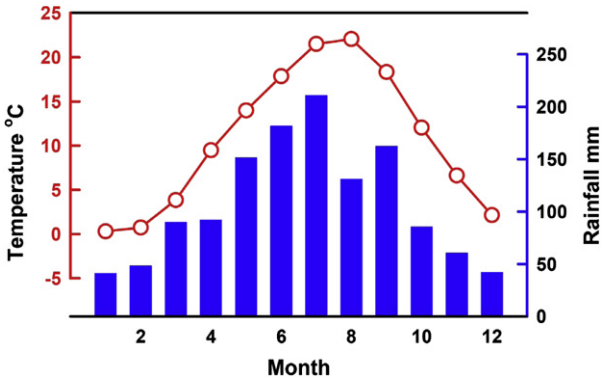

Fig. 2. Averaged monthly air temperature (circles) and rainfall (bars) records and temperature in Yuki during AD 1988–2007.

2. Materials and methods

2.1. 1Maboroshi cave and local setting

Maboroshi Cave (34°49′ N, 133°13′ E; altitude: 450 m) is located in NE Hiroshima Prefecture, Honshu Island, Japan (Fig. 1). The local mean annual rainfall during AD 1988–2007 is 1296 mm, 65% from the Pacific Ocean in summer monsoon seasons (May–September), 22% from the Japan Sea during winter monsoon seasons (November–March) and 13% from the rest of a year, as recorded at the Yuki observatory station (Fig. 2; 34°47′ N, 133°16′ E; altitude: 510 m), 5.6 km SE from Maboroshi Cave. The 20-yrs mean annual temperature is 10.7 °C.

The cave developed in Carboniferous–Permian limestone bedrock. The underground passage is mostly horizontal, partly narrow, and was filled with mud when the cave was first discovered in 1992. The present length of the explorable portion of the cave is about 740 m. A 130 mm-long stalagmite (Fig. 3a), Hiro-1, was collected 150 m from the cave entrance. The sample is 60 mm in diameter, with a straight growth axis and flat central laminae of 20–30 mm width.

2.2. Stable oxygen isotope analysis and ^{230}Th dating

Specimens were subsampled along the maximum growth axis of the stalagmite Hiro-1 for oxygen isotopic measurements by a Finnigan GASBENCH II with MAT Delta Plus GC-MS system housed at Hiroshima University (Hori et al., 2009). For a low-resolution $\delta^{18}O$ record over the whole stalagmite, powder subsamples, ~300 μg each, were extracted at 200-μm intervals along the central growth axis from a flat polished surface using a dental drill (Fig. 3a). To obtain a high-resolution $\delta^{18}O$ record during the last deglaciation, subsamples of 90–120 μg, were micro-milled with a 50-μm interval at depths from 55.75 to 80.95 mm from the top, 5.0 mm next to the low-resolution path, (Fig. 3b). Drip water samples were collected during AD 2006–2007 for $\delta^{18}O$ measurements.

$\delta^{18}O$ (‰) values were calculated with respect to the Vienna Pee Dee Belemnite (VPDB) standard for stalagmite carbonates and to the Standard Mean Ocean Water (SMOW) for drip water. Repeated measurements of laboratory standard specimens calibrated with NBS-19 confirmed that the 1-sigma standard deviation of $\delta^{18}O$ values was better than 0.1‰.

The absolute ages were determined by ^{230}Th methods (Shen et al., 2002, 2003; Frohlich et al., 2009). Nineteen subsamples (39–64 mg each) were drilled from 16 horizons of the stalagmite, Hiro-1, shown in Fig. 3b for U–Th chemistry (Shen et al., 2003) and isotopic measurements on a multi-collector inductively coupled plasma mass spectrometer (MC-ICP-MS), Thermo NEPTUNE in the High-precision Mass Spectrometry and Environment Change Laboratory (HISPEC), Department of Geosciences, National Taiwan University.

The average 2-sigma precision of the corrected ^{230}Th dates is ±70 yrs (Table 1). Duplicate ^{230}Th dates for coeval subsamples at depths, 60.8 mm, 75.0 mm, and 81.0 mm, validate the new U–Th methodology used in this study. Except for the subsample at depth 56.8 cm, ^{232}Th levels are as low as 3–500 ppt (Table 1). Corrections for initial ^{230}Th are only 3 yrs on average, much smaller than the dating errors. The chronology of the stalagmite is developed using linear interpolation between ^{230}Th dates, which are in stratigraphic order.

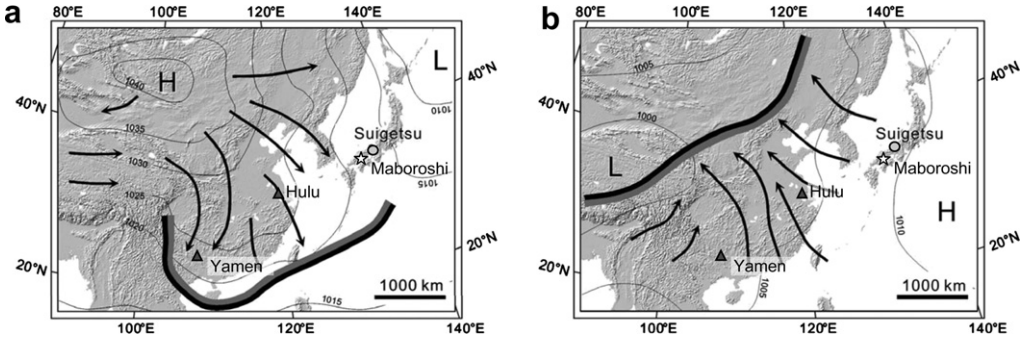

Fig. 1. Locations of Maboroshi (34°49′ N, 133°13′ E), Hulu (32°30′ N, 119°10′ E), and Yamen (25°29′ N, 107°54′ E) caves, and Lake Suigetsu (35°35′ N, 135°53′ E), in the EAM region with atmospheric circulation in (a) winter and in (b) summer. Bold lines indicate modern summer and winter monsoon fronts. Arrows show seasonal dominant wind vectors [modified from Porter and An (1995) and Nakagawa et al. (2006)].

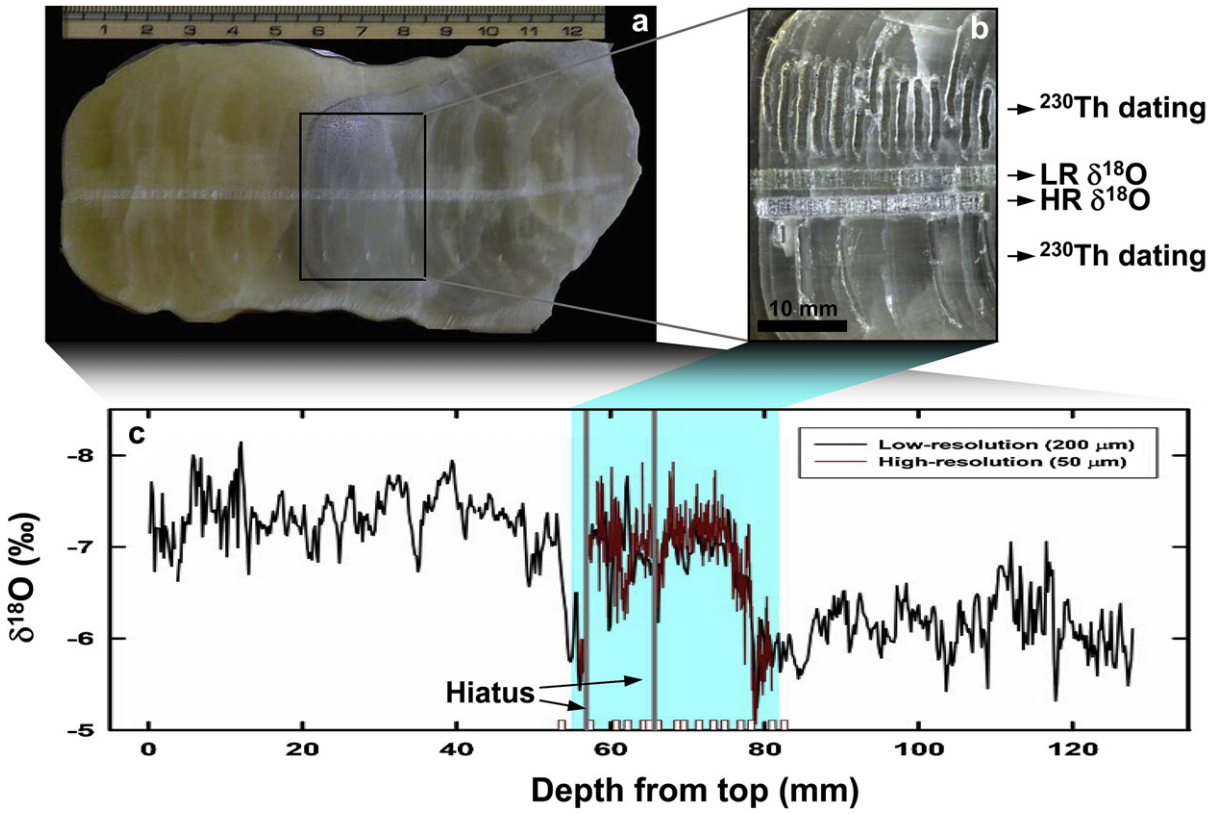

Fig. 3. The stalagmite, Hiro-1, and its $\delta^{18}O$ profiles. (a) A photo of the 13 cm-long stalagmite sample, Hiro-1. For oxygen stable isotopic measurements, subsamples with a low spatial resolution of 200 μm were drilled along the central growth axis. (b) High-resolution, 50 μm, subsamples were micro-milled from depths of 55.75–80.95 mm. Also shown are subsampling positions for ^{230}Th dating. Totally nineteen subsamples were drilled from this section. (c) Low-resolution (black line) and high-resolution (dark red line) stalagmite carbonate $\delta^{18}O$ records versus depth. Gray bars show two hiatuses and dark red hollow bars are the horizons for ^{230}Th dating. (For interpretation of the references to color in this figure legend, the reader is referred to the web version of this article).

2.3. *Calculation of atmospheric* $\Delta^{14}C$ from Lake Suigetsu

Atmospheric $\Delta^{14}C$ values in Lake Suigetsu were computed to compare with the existing radiocarbon age calibration data sets [IntCal04 (Reimer et al., 2004), marine planktonic foraminifera (Hughen et al., 2006), and fossil corals (Fairbanks et al., 2005)]. $\Delta^{14}C$ (‰) is a notation to represent the degree of deviation from the pre-industrial "modern" atmospheric value. It was originally defined in Stuiver and Polach (1977):

$$\Delta^{14}C(‰) = \left(\frac{A_{SN}}{A_{abs}} - 1\right) \times 1000(‰)$$

where A_{SN} is the normalized ^{14}C activity of the sample and A_{abs} is the specific ^{14}C activity of the absolute international standard (*i.e.* age corrected oxalic acid activity) (Stuiver and Polach, 1977). We calculated the atmospheric $\Delta^{14}C$ value of a sample when it was formed (time t_1) based on its conventional ^{14}C age and its calendar age using the following equation:

$$\Delta^{14}C(‰) \text{ at time } t_1 = \left(\frac{A_{SN}}{A_{abs}} - 1\right) \times 1000(‰)$$
$$= \left(\frac{e^{\lambda_1 \times t_1}}{e^{\lambda_c \times t_c}} - 1\right) \times 1000(‰)$$

where:

- λ_1 is the decay constant of ^{14}C based on the currently accepted ^{14}C half-life, 5730 years (Godwin, 1962).
- t_1 is the calendar age of the sample. In the case of fossil corals discussed in this study, the calendar ages of the samples were determined by ^{230}Th dating methods (Fairbanks et al., 2005; Chiu et al., 2007). The calendar age determinations of the Lake Suigetsu varve sediments were described in Kitagawa and van der Plicht (2000). In the original data table (Kitagawa and van der Plicht, 2000), a conventionally ^{14}C-dated varve sediment sample corresponds to a certain thickness in depth and a range of varve ages. In other words, the upper limit and lower limit of a conventionally ^{14}C-dated varve sediment sample were not reported by an exact calendar age assignment. In order to calculate the atmospheric $\Delta^{14}C$ values of the Lake Suigetsu record, we have taken the average value of the upper and lower limits as the calendar age of the varve sediment.
- λ_C is the decay constant of ^{14}C based on Libby's half-life, 5568 years, which has been used in the calculation of reported conventional ^{14}C ages.
- t_C is the reservoir effect-corrected conventional ^{14}C ages.

3. Results and discussion

3.1. *Maboroshi stalagmite* $\delta^{18}O$ *record*

Maboroshi stalagmites formed under oxygen isotopic equilibrium conditions with nearly 100% relative humidity and slow formation rates of 5–10 μm/yr. The average drip water $\delta^{18}O$ value is $-8.85 \pm 0.07‰$ (1σ of the mean, $1\sigma_m$). The average $\delta^{18}O$ value of $-7.38 \pm 0.13‰$ ($1\sigma_m$) in recently active stalagmites can be

Table 1
Uranium and thorium isotopic compositions and ^{230}Th ages for subsamples of stalagmite Hiro-1by MC-ICP-MS.

Depth mm	Weight g	^{238}U ppb	^{232}Th ppt	δ^{234}U measured[a]	^{230}Th/^{238}U activity ratio[c]	^{230}Th/^{232}Th × 10^{-6}[d]	Age BP uncorrected	Age BP corrected[c,e]	$\delta^{238}U_{initial}$ corrected[b]
53.8	0.0482	472.7 ± 0.6	27.6 ± 7.2	864.8 ± 2.8	0.1306 ± 0.0008	36855 ± 9,633	7827 ± 49	7,826 ± 49	884.3 ± 2.8
54.4	Hiatus								
56.8	0.0478	580.8 ± 0.9	3030.5 ± 10.4	864.4 ± 3.5	0.1778 ± 0.0009	563 ± 3	10,807 ± 60	10,734 ± 70	891.2 ± 3.6
60.8	0.0576	381.0 ± 0.6	508.5 ± 21.2	869.5 ± 4.2	0.1784 ± 0.0009	2207 ± 92	10,813 ± 63	10,794 ± 64	896.6 ± 4.3
60.8	0.0457	348.3 ± 0.2	216.1 ± 7.6	860.0 ± 2.0	0.1769 ± 0.0012	4707 ± 169	10,773 ± 76	10,765 ± 76	886.7 ± 2.1
							wt-averaged date 10,782 ± 47		
62.4	0.0350	459.6 ± 0.3	222.0 ± 10.1	851.6 ± 2.1	0.1794 ± 0.0010	6131 ± 280	10,986 ± 66	10,979 ± 66	878.5 ± 2.2
64.4	0.0384	241.0 ± 0.2	3.0 ± 9.1	840.3 ± 3.3	0.1812 ± 0.0016	237,256 ± 707,877	11,174 ± 106	11,174 ± 106	867.4 ± 3.4
65.0	0.0452	286.6 ± 0.4	58.6 ± 7.7	837.5 ± 4.0	0.1840 ± 0.0012	14,856 ± 1,956	11,376 ± 84	11,373 ± 84	865.0 ± 4.1
65.4	Hiatus								
65.7	0.0328	432.2 ± 0.3	20.6 ± 10.6	827.5 ± 2.6	0.2020 ± 0.0012	69,869 ± 35,941	12,625 ± 82	12,624 ± 82	857.7 ± 2.7
68.6	0.0453	407.3 ± 0.7	36.9 ± 7.7	822.1 ± 3.7	0.2055 ± 0.0010	37,439 ± 7,796	12,896 ± 71	12,895 ± 71	852.8 ± 3.8
69.8	0.0373	391.4 ± 0.4	96.5 ± 9.3	832.3 ± 2.6	0.2118 ± 0.0012	14,181 ± 1,374	13,239 ± 82	13,235 ± 82	864.1 ± 2.7
71.6	0.0450	455.4 ± 0.5	5.6 ± 7.7	844.7 ± 2.8	0.2175 ± 0.0011	291,106 ± 400,907	13,514 ± 78	13,514 ± 78	877.7 ± 3.0
73.6	0.0393	515.5 ± 0.6	8.3 ± 8.9	836.7 ± 3.1	0.2167 ± 0.0012	223,042 ± 238,866	13,526 ± 82	13,526 ± 82	869.4 ± 3.2
75.0	0.0635	426.6 ± 0.6	18.2 ± 5.5	831.5 ± 3.4	0.2177 ± 0.0008	84,444 ± 25,507	13,635 ± 62	13,634 ± 62	864.3 ± 3.6
75.0	0.0458	401.4 ± 0.4	3.4 ± 7.6	834.2 ± 2.7	0.2170 ± 0.0011	425,831 ± 958,292	13,563 ± 75	13,563 ± 75	867.0 ± 2.8
							wt-averaged date 13,605 ± 49		
77.2	0.0526	533.9 ± 0.9	17.2 ± 6.6	853.1 ± 3.5	0.2317 ± 0.0008	118,836 ± 45,739	14,386 ± 62	14,386 ± 62	888.7 ± 3.7
78.6	0.0396	604.8 ± 0.4	465.9 ± 8.8	848.5 ± 2.1	0.2359 ± 0.0009	5,056 ± 98	14,701 ± 65	14,690 ± 65	884.6 ± 2.2
81.0	0.0632	640.2 ± 1.2	104.3 ± 5.7	865.7 ± 4.0	0.2516 ± 0.0010	25,509 ± 1,388	15,590 ± 74	15,588 ± 74	904.8 ± 4.2
81.0	0.0477	701.4 ± 0.5	137.1 ± 7.3	865.4 ± 2.3	0.2510 ± 0.0008	21,210 ± 1,133	15,554 ± 58	15,551 ± 58	904.4 ± 2.4
							wt-averaged date 15,565 ± 49		
82.6	0.0407	775.6 ± 0.5	11.9 ± 8.6	807.9 ± 2.1	0.2461 ± 0.0008	264,192 ± 189,410	15,752 ± 56	15,752 ± 56	844.8 ± 2.2

Chemistry was performed during AD 2007–2009 (Shen et al., 2003) and instrumental analyses on MC-ICP-MS (Frohlich et al., 2009).
Analytical errors are 2s of the mean.

[a] $\delta^{234}U = ([^{234}U/^{238}U]_{activity} - 1) \times 1000$.

[b] δ^{234}U corrected was calculated based on ^{230}Th age (T), i.e., $\delta^{234}U_{initial} = \delta^{234}U_{measured} \times e^{\lambda 234 * T}$, and T is corrected age.

[c] $[^{230}Th/^{238}U]_{activity} = 1 - e^{-\lambda_{230}T} + (\delta^{234}U/1000)[\lambda_{230}/(\lambda_{230} - \lambda_{234})](1 - e^{-(\lambda_{230}-\lambda_{234})T})$, where T is the age. Decay constants are 9.1577 × 10^{-6} yr^{-1} for 230Th, 2.8263 × 10^{-6} yr^{-1} for ^{234}U (Cheng et al., 2000), and 1.55125 × 10^{-10} yr^{-1} for ^{238}U (Jaffey et al., 1971).

[d] The degree of detrital ^{230}Th contamination is indicated by the ^{230}Th/^{232}Th atomic ratio instead of the activity ratio.

[e] Age (before AD 1950) corrections were made using a ^{230}Th/^{232}Th atomic ratio of 4 ± 2 ppm, which is the value for material at secular equilibrium with the crustal ^{232}Th/^{238}U value of 3.8 and an arbitrarily assumed uncertainty of 50%.

interpreted as precipitation at equilibrium within a temperature range of 10.3–11.7 °C (Craig et al., 1963), consistent with the modern annual temperature of 10.7 °C at this site. The stalagmite Hiro-1 δ^{18}O record also passes the duplication test with another parallel δ^{18}O profile (Fig. 3c) and the Hendy Test (Fig. 4) (Hendy, 1971) with coeval subsamples at four depths.

The Maboroshi δ^{18}O values range from −5 to −8‰ for the whole time interval of 15.5–10.7 ka and fluctuate between −6.4 and −5.0‰ during 15.5–14.7 ka (Supplementary data; Fig. 5b). Following an abrupt decrease of ~1.7‰ at the t-BA, the values maintain between −6.5 and −7.5‰ during the BA, with a short δ^{18}O enrichment (0.5‰) event at ~14.0 ka, corresponding to the Older Dryas (OD). The δ^{18}O record then shows a distinct increase of ~1.0‰ at the t-YD before a depositional hiatus from 12.6 to 11.4 ka. After the hiatus, the δ^{18}O values stay at ~−7‰ with a positive shift of ~0.5‰ at 11.0–10.9 ka. Over this 4.8-kyr time interval, the influence of a 50-m sea level rise (Cutler et al., 2003) produced a slight decrease in seawater δ^{18}O at a rate of −0.088‰/kyr due to ice melting (Schrag et al., 1996).

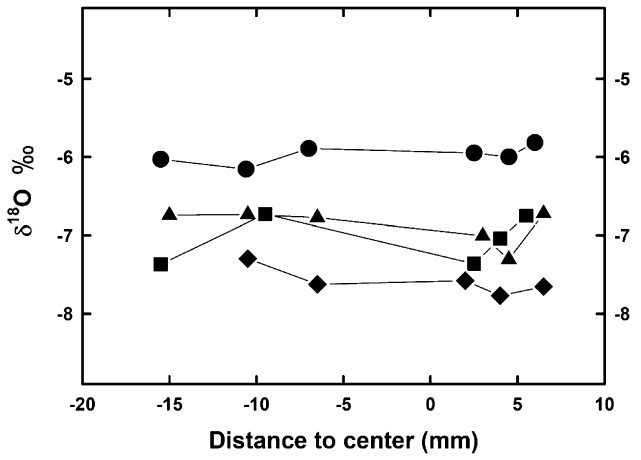

Fig. 4. Hendy Test of δ^{18}O for coeval subsamples of four layers at depths, 56.6 mm (circles), 57.6 mm (squares), 67.7 mm (diamonds), and 77.8 mm (triangles), spanning 21.5 mm over the interval for high-resolution δ^{18}O record.

The variations in the δ^{18}O records in the Chinese caves have been considered to reflect the relative changes of the summer and winter precipitations (Wang et al., 2001) or just the summer precipitation for simplicity, and thus relate to summer EAM variability (Yuan et al., 2004; Wang et al., 2008). Stalagmite δ^{18}O variability in Maboroshi Cave is unlikely to reflect the same factors as Chinese caves for the following reasons. (1) Unlike Mainland China, there are two major moisture sources for Japan. One is the Pacific Ocean during summer and the other is the Japan Sea during winter. (2) A clear seasonal difference in rainfall d^{18}O values in Mainland China is obscure in Japan. For example, at the Hulu Cave site, the recorded δ^{18}O values of the summer monsoon range from −9 to −13‰, and its principal moisture source from the Pacific Ocean contributes 80% of the annual precipitation. The winter monsoon brings the rest of the annual precipitation with much higher δ^{18}O values of −3‰ to +2‰ (Wang et al., 2001). On the other hand, at Nagaya (34°47′ N, 133°28′ E), 22 km east of Maboroshi Cave, seasonal variation in rainfall δ^{18}O values was insignificant during AD 2005–2007 (Hori et al., 2009). The summer value was −8.4 ± 2.1‰ (1σ) and the winter value was −9.0 ± 3.0‰ (1σ) during that period (Hori et al., 2009). Monthly rainfall δ^{18}O values at Ryori and Tokyo, Global Network of Isotopes in Precipitation (GNIP) sites in Japan, do not show clear seasonal variations, either (Fig. 6). (3)

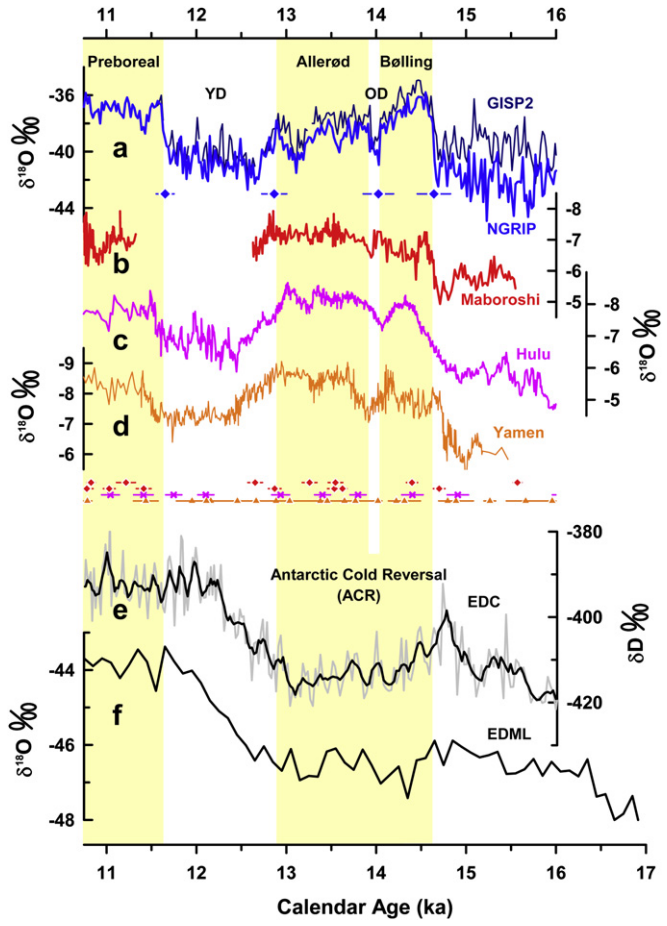

Fig. 5. Deglacial proxy records from Greenland, Japanese and Chinese caves, and Antarctica. (a) $\delta^{18}O$ records of Greenland ice cores, NGRIP (blue) and GISP2 (dark blue) [GICC05 timescale (NGRIP, 2006)]. The error bars indicate 2-sigma age uncertainties. (b) Maboroshi stalagmite Hiro-1 $\delta^{18}O$, Japan. (c) Hulu stalagmite H82 $\delta^{18}O$, China (Wang et al., 2001). (c) Yamen stalagmite Y1 $\delta^{18}O$, China (Yang et al., 2010). The ^{230}Th ages and errors are color-coded by stalagmites. (e) Antarctic ice δD for the European Project for Ice Coring in Antarctica (EPICA) Dome C (EDC) core (Jouzel et al., 2007) [adjusted EDC3 age model (Barker et al., 2009)]. Gray line is for raw data and solid line for the 5-point running averages. (f) Antarctic ice $\delta^{18}O$ for the EPICA Dronning Maud Land (EDML) core (GICC05 age model) (EPICA, 2006). Shaded bands represent periods of warmth, Bølling, Allerød, and Preboreal, in Greenland. (For interpretation of the references to color in this figure legend, the reader is referred to the web version of this article).

The so-called "amount effect", the observed decrease in rainfall $\delta^{18}O$ values followed by increased amounts of rainfall, is −1.2 to −3.6‰/100 mm in rainfall for the low-latitude intertropical convergence zone (ITCZ) (Dansgaard, 1964; Rozanski et al., 1993; Lachniet, 2009). This effect appears to be −0.26‰/100 mm at Ryori and −0.35‰/100 mm at Tokyo (Fig. 7), which is 4–10 times less than that in the ITCZ (Lachniet, 2009). The facts of the existence of a major winter moisture source from the Japan Sea, the absence of seasonal variation in rainfall $\delta^{18}O$ values, and a weak "amount effect" suggest that the scenario for the Maboroshi $\delta^{18}O$ record at the eastern site is different from those of Chinese caves (Wang et al., 2001, 2005; Yang et al., 2010). Hence the interpretation primarily based on the precipitation intensity for Chinese cave records cannot be directly applied to the Maboroshi stalagmite record. In order to compare the two records we need to first consider the factors responsible for $\delta^{18}O$ variability at Maboroshi cave.

Meteorological observations show that the northwest Pacific air mass dominates Japanese summer temperature and the southward Siberian air mass controls the regional winter temperature (cf.

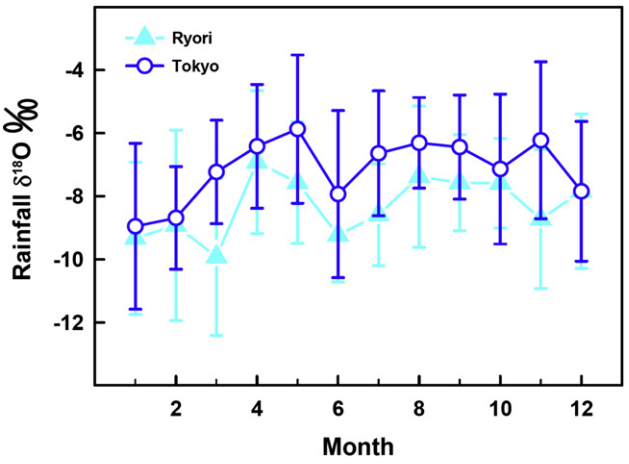

Fig. 6. Monthly-mean rainfall $\delta^{18}O$ data ($\pm 1\sigma$) for Ryori (39°02′ N, 141°49′ E) from AD 1979–2005 (triangles) and Tokyo (35°41′ N, 139°46′ E) from AD 1961–1979 (circles) [Global Network of Isotope in Precipitation, GIS Global Mapping System for Isotopes in the Water Cycle, International Atomic Energy Agency (http://www.iaea.org/water/)].

Nakagawa et al., 2006). The most distinct feature of the measured stalagmite $\delta^{18}O$ values is a ~1.7‰ decrease in a 160-yrs time interval during the t-BA (Fig. 5b). A first-order estimate of a 4 ± 1 °C warming during this time (Nakagawa et al., 2003, 2006) (Fig. 8c) approximately corresponds to a 1.0‰ decrease in $\delta^{18}O$. The residual is likely attributed to changes in rainfall amount, moisture source and isotopic fractionation associated with atmospheric transport. Furthermore, temperature rise might cause an opposite effect to elevate $\delta^{18}O$ values in local meteoric water. Taken together, the Maboroshi $\delta^{18}O$ record is suggested to qualitatively reflect past changes in the relative intensity of summer and winter monsoons at the site.

Climate events in the Maboroshi record, from the easternmost front of the EAM, are aligned with those in the Hulu (Wang et al., 2001) and Yamen (Yang et al., 2010) cave records, from central and southern China, within dating errors (Fig. 5). This coherence indicates that the strength of the EAM is broadly controlled by common forcings. Regional dissimilarities appear in the high-frequency domain with decadal variability influenced by differences in hydrological and aquifer dynamics. The 1.2-kyr hiatus in

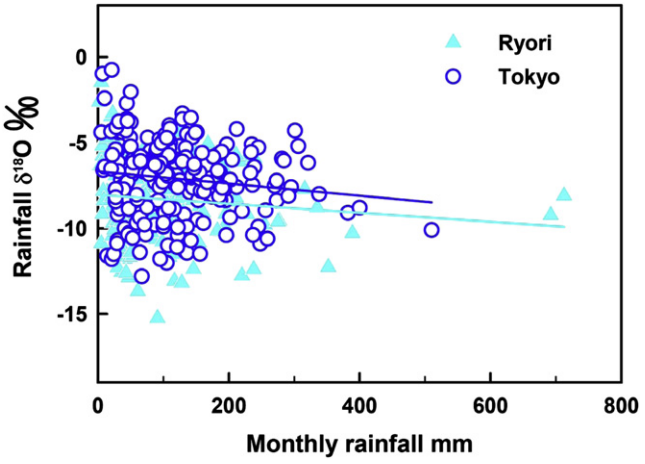

Fig. 7. Plot of rainfall water $\delta^{18}O$ versus the amount of monthly rainfall amount and their regression lines for Ryori (triangles) and Tokyo (circles) [Global Network of Isotope in Precipitation, GIS Global Mapping System for Isotopes in the Water Cycle, International Atomic Energy Agency (http://www.iaea.org/water/)].

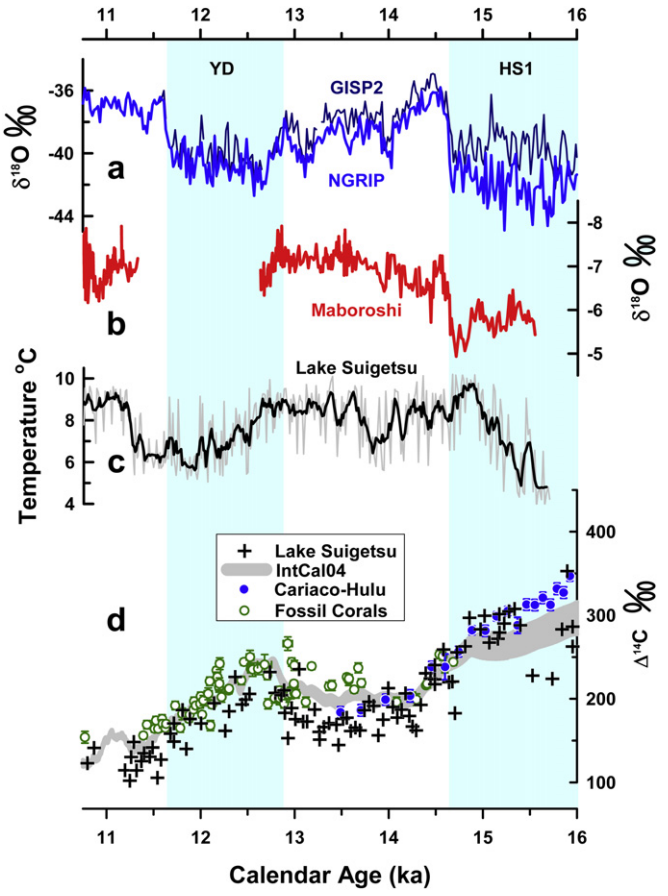

Fig. 8. Deglacial records of Greenland ice core $\delta^{18}O$, Japanese cave and lake, and atmospheric $\Delta^{14}C$. (a) $\delta^{18}O$ records of Greenland ice cores, NGRIP (blue) and GISP2 (dark blue) [GICC05 timescale (NGRIP, 2006)]. (b) Maboroshi stalagmite Hiro-1 $\delta^{18}O$. (c) Lake Suigetsu pollen-inferred air temperature (Nakagawa et al., 2003) (varve-counted and floating chronology). Gray and solid lines indicate the raw data and 5-point running average records, respectively. (d) Atmospheric radiocarbon activity records inferred from Lake Suigetsu (black) and other calendrical records from IntCal04 (Reimer et al., 2004) (gray), Cariaco Basin foraminifera (Hughen et al., 2006) (blue) (^{230}Th-dated Hulu Cave timescale), and fossil corals (Fairbanks et al., 2005) (green) (^{230}Th chronology). Shaded bands represent cold periods in Greenland, HS1 and YD. (For interpretation of the references to color in this figure legend, the reader is referred to the web version of this article).

the Maboroshi record during the YD might have been caused by extremely low summer precipitation in East Asia at that time (Cai et al., 2009). However, in the Lake Suigetsu pollen records (Nakagawa et al., 2006), the YD precipitation was only slightly lower in summer and even higher in winter than during the BA. This hiatus could simply result from a local discontinuity in the percolating drip water above the stalagmite.

3.2. Asian summer monsoon during the last deglaciation

The overall cave-inferred EAM events resemble those in Greenland ice-core records (Fig. 5). During the cold Heinrich stadial 1 (HS1) (Broecker and Barker, 2007; Barker et al., 2009), the disruption of the Atlantic meridional overturning circulation (AMOC) (McManus et al., 2004; Marchitto et al., 2007; Mangini et al., 2010; Shakun and Carlson, 2010), caused by insolation-driven melt water (Cheng et al., 2009), hindered the northward transport of heat from low latitudes and the Southern Hemisphere (SH) (EPICA, 2006). At that time, temperatures in the SH, including the Southern Ocean (Lamy et al., 2007; Barker et al., 2009) and Antarctica (EPICA, 2006; Jouzel et al., 2007), increased (Fig. 5e, f) and the northern westerlies would be expected to move southward (Anderson et al., 2009). Under these conditions, the mean position of the ITCZ would lay south of its current position, producing an asymmetric Hadley circulation and weakened summer EAM (Wang et al., 2001, 2005; Yang et al., 2010) as well as enhanced winter EAM (Nakagawa et al., 2006).

High-resolution ice-core analyses show that at the onset of the BA warming event occurred as an abrupt heat migration from the SH to the Northern Hemisphere (NH), causing a rapid temperature increase within 1–3 years in Greenland's moisture source region (Steffensen et al., 2008). At the same time, a northward shift of the ITCZ intensified the summer EAM. Greenland temperatures increased accordingly (Fig. 5a) due to the enhanced advection of moisture and northward heat transport (Steffensen et al., 2008).

The reduction in the summer EAM at the onset of the YD reflects different circumstances. It has been proposed that a slowdown or reduction of the AMOC occurred after a pronounced increase of fresh melt water into the North Atlantic Ocean (McManus et al., 2004; Marchitto et al., 2007; Mangini et al., 2010; Shakun and Carlson, 2010). The resultant cooling observed in Greenland ice cores (Fig. 5a) caused an intensified Siberian High (Nakagawa et al., 2006), an altered Hadley cell, and a southward shift of the ITCZ (Wang et al., 2004; Stouffer et al., 2006). These conditions led to decreased temperatures in Japan (Nakagawa et al., 2006) and reduced precipitation in China (Wang et al., 2001; Yang et al., 2010) (Fig. 5).

3.3. Decoupling of $\delta^{18}O$ records of Asian caves and Greenland during the BA

During the BA, distinctly different climatic trends are observed in the $\delta^{18}O$ records of eastern Asian caves and Greenland ice cores (Fig. 5). Our results demonstrate a 0.6‰ decrease in $\delta^{18}O$ at Maboroshi, comparable to a 0.5‰ decrease at Hulu and a 0.7‰ decrease at Yamen. Up to 0.2–0.3‰ of the observed $\delta^{18}O$ changes can be attributed to the concurrent 20–30-m sea level rise during the BA (Schrag et al., 1996; Cutler et al., 2003), but the remaining 0.2–0.5‰ decrease is best explained as a result of intensified summer EAM activity. In contrast, ice-core $\delta^{18}O$ data indicate a temperature maximum at the beginning of the Bølling, followed by a thermal decline in the northern high latitudes throughout the BA.

It has been suggested that following the t-BA, a reorganization of the prevailing atmospheric circulation (Steffensen et al., 2008) enhanced the northward advection of moisture and heat, resulting in increased Greenland temperatures (Anderson et al., 2009). In this case, southern westerlies would migrate northward (Anderson et al., 2009; Denton et al., 2010), resulting in SH cooling (Barker et al., 2009; Divine et al., 2010). Such a climate pattern is consistent with the proposed interhemispheric bipolar seesaw mechanism that controls global climate over long time periods (Stocker and Johnsen, 2003). This situation was noted early by An (2000), who argued that a strengthened winter Australian monsoon would enhance cross-equatorial transport of moisture and heat from low latitudinal oceans, including the Indian Ocean and South China Sea, to East Asia and move the ITCZ northward. The net effect of these conditions produces the intensification of the summer EAM.

Modern decadal observatory streamline data (Kalnay et al., 1996; Nguyen and McGregor, 2009) show that during austral winters, strong southeasterly winds produced by the Australian High turn northwestward after crossing the equator. This humid and warm cross-equatorial flow strengthens the summer EAM. A four-centennial coral proxy network in the Indian Ocean demonstrates this intensification of northwestward cross-equatorial flow and the enhancement of the EAM during the 1600s–1900s (Gong and Luterbacher, 2008). Our cave-inferred summer EAM record over

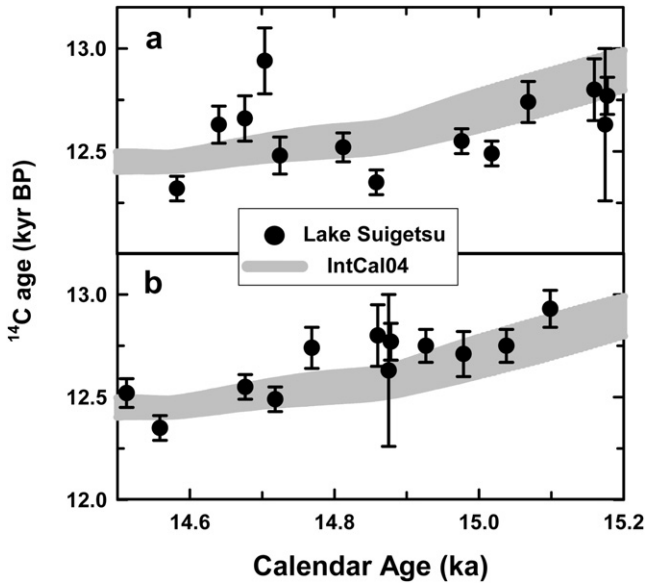

Fig. 9. Relationship between ^{14}C age and calendar age during 15.2–14.5 ka. (a) Records of IntCal04 (Reimer et al., 2004) (gray) and Lake Suigetsu (black) (varve-counted and floating chronology) (Nakagawa et al., 2003). (b) Records of IntCal04 (Reimer et al., 2004) (gray) and Lake Suigetsu (Nakagawa et al., 2003) with minus 250-yr adjustment (black) (^{230}Th-dated Maboroshi Cave timescale; this study).

the entire BA (Fig. 5) could have been controlled by such a "pressure push" [Fig. 1 of An, 2000] cross-equatorial forcing, originating from the cold SH (Jouzel et al., 2007; Barker et al., 2009; Divine et al., 2010). Decoupling between summer EAM and Greenland temperatures observed during Interstadials 8, 12, and 16/17 could also have resulted from the same mechanism [Fig. 5 of Svensson et al., 2008].

3.4. Correction for Lake Suigetsu chronology

The floral assemblage-inferred temperature change record from Lake Suigetsu is apparently asynchronous with the Maboroshi and Greenland records (Fig. 8). The warming observed at ~15.3 ka in the Lake Suigetsu record predates the Greenland t-BA by about five centuries, while a lake cold event during 12.3–11.3 ka postdates the Greenland YD event by ~300 yrs. A dynamic vegetation climate response would be too slow (Li et al., 2009) to account for the 300-yrs disparity around the YD, and conflicts with the 500-yrs difference between the Greenland t-BA and the preceding warming observed in the Lake Suigetsu. An offset of ~30‰ in Δ^{14}C values is observed between the lake values and contemporaneous values from IntCal04 (Reimer et al., 2004), marine planktonic foraminifera (Hughen et al., 2006) and fossil corals (Fairbanks et al., 2005) during the time interval 14.5–11.0 ka (Fig. 8d). The absolute-dated Maboroshi stalagmite δ^{18}O record provides a means to correct for the apparent temporal inconsistencies in the Lake Suigetsu varve record, analogous to the approach taken to correct the Cariaco Basin varved sediment record using stalagmite results from Hulu Cave (Hughen et al., 2006).

A direct correction can be made to the Lake Suigetsu record through comparing the two time-series. Both the Maboroshi and Lake Suigetsu records show a broad plateau throughout the BA period, and the most distinctive point within this time range is at the end of t-BA, where cave δ^{18}O data peak at 14.5 ka (Fig. 8). This serves as an anchoring point to adjust the Lake Suigetsu chronology. A correction of −250 years can be reasonably applied to adjust the lake calendar ages between 15.2 and 14.5 ka (Fig. 9). The corrected Lake Suigetsu curve is more consistent with the IntCal04 dataset (Reimer et al., 2004) for this time range, which verifies our revision for Lake Suigetsu chronology over this time period (Fig. 9).

4. Conclusions

To better understand the influence of high-latitudinal forcings on the EAM and asynchronous climate sequences inferred from Lake Suigetsu sediments and Greenland ice cores during Termination I, a decadally-resolved stalagmite δ^{18}O record of regional climate signals from Maboroshi Cave was produced. Comparison of precise absolute-dated Japanese and Chinese stalagmite δ^{18}O records indicates synchroneity of cave-inferred regional climate events in the same EAM regime. This study shows that the EAM has been influenced by high-latitudinal forcings not only from NH, but also from SH during the last deglaciation. Decoupled from decreasing temperatures in Greenland during the BA, the concurrent intensified EAM is likely attributed to a strong cross-equatorial flow, resulted from a cold SH and northward southern westerlies according to the bipolar seesaw mechanism. Our results provide a firm chronological framework to resolve temporal ambiguities in the Lake Suigetsu paleoclimate record for the period studied. We expect a complete chronology for Lake Suigetsu through ongoing studies employing cross-correlation of multiple lake sediment cores (Nakagawa et al., 2009; www.suigetsu.org). From the evidence presented in the Maboroshi record, the questions of climatic asynchroneity between Japan and the North Atlantic are dismissed.

Acknowledgements

We are grateful to Y. Tsuchiya for guidance in sampling the cave deposits and giving permission to collect the stalagmite and to T. Nakagawa for generously offering Lake Suigetsu data. We thank K. Fukumura, T. Togo, K. Ohmori, and S. Suzuki for their support in the field and laboratory. Discussions with R.L. Edwards of the University of Minnesota and H.-H. Hsu of the Department of Atmospheric Sciences, National Taiwan University were very helpful. Constructive reviews by A. Gupta and one anonymous reviewer significantly improved this paper. This study was supported by grants from the Japanese Ministry of Education and Science (17340150 and 21340149 to A.K.) and Taiwan ROC National Science Council (96-2752-M002-012-PAE, 98-2116-M-002-006 and 98-2661-M-002-012 to C.-C.S.).

Appendix. Supplementary data

Supplementary data can be founded with this article in the online version at doi:10.1016/j.quascirev.2010.08.012.

References

An, Z., 2000. The history and variability of the East Asian paleomonsoon climate. Quaternary Science Reviews 19, 171–187.

Anderson, R.F., Ali, S., Bradtmiller, L.I., Nielsen, S.H.H., Fleisher, M.Q., Anderson, B.E., Burckle, L.H., 2009. Wind-driven upwelling in the southern ocean and the deglacial rise in atmospheric CO_2. Science 323, 1443–1448.

Barker, S., Diz, P., Vautravers, M.J., Pike, J., Knorr, G., Hall, I.R., Broecker, W.S., 2009. Interhemispheric Atlantic seesaw response during the last deglaciation. Nature 457, 1097–1103.

Broecker, W., Barker, S., 2007. A 190‰ drop in atmosphere's Δ^{14}C during the "Mystery Interval" (17.5 to 14.5 kyr). Earth and Planetary Science Letters 256, 90–99.

Cai, B., Edwards, R.L., Cheng, H., Tan, M., Wang, X., Liu, T., 2009. A dry episode during the Younger Dryas and centennial-scale weak monsoon events during the early Holocene: a high-resolution stalagmite record from southeast of the Loess Plateau, China. Geophysical Research Letters 35. doi:10.1029/2007GL030986 L02705.

Cai, Y., An, Z., Cheng, H., Edwards, R.L., Kelly, M.J., Liu, W., Wang, X., Shen, C.-C., 2006. High-resolution absolute-dated Indian Monsoon record between 53 and 36 ka from Xiaobailong Cave, Southwestern China. Geology 34, 621–624.

Cheng, H., Edwards, R.L., Hoff, J., Gallup, C.D., Richards, D.A., Asmersom, Y., 2000. The half-lives of uranium-234 and thorium-230. Chemical Geology 169, 17–33.
Cheng, H., Edwards, R.L., Wang, Y.J., Kong, X.G., Ming, Y.F., Kelly, M.J., Wang, X.F., Gallup, C.D., Liu, W.G., 2006. A penultimate glacial monsoon record from Hulu Cave and two-phase glacial terminations. Geology 34, 217–220.
Cheng, H., Edwards, R.L., Broecker, W.S., Denton, G.H., Kong, X., Wang, Y., Zhang, R., Wang, X., 2009. Ice age terminations. Science 326, 248–252.
Chiu, T.-C., Fairbanks, R.G., Cao, L., Mortlock, R.A., 2007. Analysis of the atmospheric ^{14}C record spanning the past 50,000 years derived from high-precision $^{230}Th/^{234}U/^{238}U$, $^{231}Pa/^{235}U$ and ^{14}C dates on fossil corals. Quaternary Science Reviews 26, 18–36.
Clemens, S., Prell, W., Murray, D., Shimmield, G., Weedon, G., 1991. Forcing mechanisms of the Indian-Ocean monsoon. Nature 353, 720–725.
Craig, H., Gordon, L.I., Horibe, Y., 1963. Isotopic exchange effects in the evaporation of water, 1, low temperature results. Journal of Geophysical Research 68, 5079–5087.
Cutler, K.B., Edwards, R.L., Taylor, F.W., Cheng, H., Adkins, J., Gallup, C.D., Cutler, P.M., Burr, G.S., Bloom, A.L., 2003. Rapid sea-level fall and deep-ocean temperature change since the last interglacial period. Earth and Planetary Science Letters 206, 253–271.
Dansgaard, W., 1964. Stable isotopes in precipitation. Tellus 16, 436–468.
Denton, G.H., Anderson, R.F., Toggweiler, J.R., Edwards, R.L., Schaefer, J.M., Putnam, A.E., 2010. The last glacial termination. Science 328, 1652–1656.
Divine, D.V., Koç, N., Isaksson, E., Nielsen, S., Crosta, X., Godtliebsen, F., 2010. Holocene Antarctic climate variability from ice and marine sediment cores: insights on ocean–atmosphere interaction. Quaternary Science Reviews 29, 303–312.
EPICA Community Members, 2006. One-to-one coupling of glacial climate variability in Greenland and Antarctica. Nature 444, 195–198.
Fairbanks, R.G., Mortlock, R.A., Chiu, T.-C., Cao, L., Kaplan, A., Guilderson, T.P., Fairbanks, T.W., Bloom, A.L., Grootes, P.M., Nadeau, M.J., 2005. Radiocarbon calibration curve spanning 0–50,000 years BP based on paired Th-230/U-234/U-238 and C-14 dates on pristine corals. Quaternary Science Reviews 24, 1781–1796.
Frohlich, C., Hornbach, M.J., Taylor, F.W., Shen, C.-C., Moala, A., Morton, A.E., Kruger, J., 2009. Huge erratic boulders in Tonga deposited by a prehistoric tsunami. Geology 37, 131–134.
Godwin, H., 1962. Half-life of radiocarbon. Nature 195, 984.
Gong, D.-Y., Luterbacher, J., 2008. Variability of the low-level cross-equatorial jet of the western Indian Ocean since 1660 as derived from coral proxies. Geophysical Research Letters 35. doi:10.1029/2007GL032409 L01705.
Hendy, C.H., 1971. The isotopic geochemistry of speleothem: part 1, the calculation of the effects of different modes of formation on the isotopic composition of speleothems and their applicability as palaeoclimatic indicators. Geochimica et Cosmochimica Acta 35, 801–824.
Heusser, L., Morley, J., 1997. Monsoon fluctuations over the past 350 kyr: high-resolution evidence from northeast Asia northwest Pacific climate proxies (marine pollen and radiolarians). Quaternary Science Reviews 16, 565–581.
Hori, M., Kawai, T., Matsuoka, J., Kano, A., 2009. Intra-annual perturbations of stable isotopes in tufas: effects of hydrological processes. Geochimica et Cosmochimica Acta 73, 1684–1695.
Huang, C.-Y., Liew, P.-M., Zhao, M., Chang, T.-C., Kuo, C.-M., Chen, M.-T., Wang, C.-H., Zheng, L.-F., 1997. Deep sea and lake records of the Southeast Asian paleomonsoons for the last 25 thousands years. Earth and Planetary Science Letters 146, 59–72.
Hughen, K., Southon, J., Lehman, S., Bertrand, C., Turnbull, J., 2006. Marine-derived ^{14}C calibration and activity record for the past 50,000 years updated from the Cariaco Basin. Quaternary Science Reviews 25, 3216–3227.
Jaffey, A.H., Flynn, K.F., Glendenin, L.E., Bentley, W.C., Essling, A.M., 1971. Precision measurement of half-lives and specific activities of U-235 and U-238. Physical Reviews 4, 1889–1906.
Jouzel, J., Masson-Delmotte, V., Cattani, O., Dreyfus, G., Falourd, S., Hoffmann, G., Minster, B., Nouet, J., Barnola, J.M., Chappellaz, J., Fischer, H., Gallet, J.C., Johnsen, S., Leuenberger, M., Loulergue, L., Luethi, D., Oerter, H., Parrenin, F., Raisbeck, G., Raynaud, D., Schilt, A., Schwander, J., Selmo, E., Souchez, R., Spahni, R., Stauffer, B., Steffensen, J.P., Stenni, B., Stocker, T.F., Tison, J.L., Werner, M., Wolff, E.W., 2007. Orbital and Millennial Antarctic climate variability over the past 800,000 years. Science 317, 793–796.
Kalnay, E., Kanamitsu, M., Kistler, R., Collins, W., Deaven, D., Gandin, L., Iredell, M., Saha, S., White, G., Woollen, J., Zhu, Y., Chelliah, M., Ebisuzaki, W., Higgins, W., Janowiak, J., Mo, K.C., Ropelewski, C., Wang, J., Leetmaa, A., Reynolds, R., Jenne, R., Joseph, D., 1996. The NCEP/NCAR 40-year reanalysis project. Bulletin of the American Meteorological Society 77, 437–471.
Kitagawa, H., van der Plicht, J., 2000. Atmospheric radiocarbon calibration beyond 11,900 cal BP from Lake Suigetsu laminated sediments. Radiocarbon 42, 370–381.
Lachniet, M.S., 2009. Climatic and environmental controls on speleothem oxygen-isotope values. Quaternary Science Reviews 28, 412–432.
Lamy, F., Kaiser, J., Arz, H.W., Hebbeln, D., Ninnemann, U., Timm, O., Timmermann, A., Toggweiler, J.R., 2007. Modulation of the bipolar seesaw in the southeast pacific during Termination 1. Earth and Planetary Science Letters 259, 400–413.
Li, Y., Harrison, S.P., Zhao, P., Ju, J., 2009. Simulations of the impacts of dynamic vegetation on interannual and interdecadal variability of Asian summer monsoon with modern and mid-Holocene orbital forcings. Global and Planetary Change 66, 235–252.
Mangini, A., Godoy, J.M., Godoy, M.L., Kowsmann, R., Santos, G.M., Ruckelshausen, M., Schroeder-Ritzrau, A., Wacker, L., 2010. Deep sea corals off Brazil verify a poorly ventilated southern pacific Ocean during H2, H1 and the Younger Dryas. Earth and Planetary Science Letters 293, 269–276.
Marchitto, T.M., Lehman, S.J., Ortiz, J.D., Flückiger, J., van Geen, A., 2007. Marine radiocarbon evidence for the mechanism of deglacial atmospheric CO_2 rise. Science 316, 1456–1459.
McManus, J.F., Francois, R., Gherardi, J.-M., Keigwin, L.D., Brown-Leger, S., 2004. Collapse and rapid resumption of Atlantic meridional circulation linked to deglacial climate changes. Nature 428, 834–837.
Morley, J.J., Heusser, L.E., 1997. Role of orbital forcing in East Asian monsoon climates during the last 350 kyr: evidence from terrestrial and marine climate proxies from core RC14-99. Paleoceanography 12, 483–493.
Nakagawa, T., Kitagawa, H., Yasuda, Y., Tarasov, P.E., Nishida, K., Gotanda, K., Sawai, Y., Yangtze River Civilization Program Members, 2003. Asynchronous climate changes in the North Atlantic and Japan during the last termination. Science 299, 688–691.
Nakagawa, T., Tarasov, P.E., Kitagawa, H., Yasuda, Y., Gotanda, K., 2006. Seasonally specific responses of the East Asian monsoon to deglacial climate changes. Geology 34, 521–524.
Nakagawa, T., Bronk-Ramsey, C., Bryant, C., Staff, R., Brock, F., Lamb, H., Brauer, A., Marshall, M., Schlolaut, G., Yokoyama, Y., Tarasov, P., Payne, R.L., Pearson, E.J., Haraguchi, T., Yonenobu, H., Tada, R., Tyler, J.J., Gotanda, K., Kossler, A., Demske, D., Takemura, K., 2009. Lake Suigetsu 2006 Varved Sediment Project – towards a purely terrestrial radiocarbon calibration model. American Geophysical Union, Fall Meeting, #PP13F-01.
NGRIP dating group, 2006. Greenland Ice Core Chronology 2005 (GICC05). In: IGBP PAGES/World Data Center for Paleoclimatology, Data Contribution Series # 2006-118. NOAA/NCDC Paleoclimatology Program, Boulder, CO, USA.
Nguyen, K.C., McGregor, J.L., 2009. Modelling the Asian summer monsoon using CCAM. Climate Dynamics 32, 219–236.
Porter, S.C., An, Z., 1995. Correlation between climate events in the North Atlantic and China during the last deglaciation. Nature 375, 305–308.
Prell, W.L., Kutzbach, J.E., 1992. Sensitivity of the Indian monsoon to forcing parameters and implications for its evolution. Nature 360, 647–652.
Reimer, P.J., Baillie, M.G.L., Bard, E., Bayliss, A., Beck, J.W., Bertrand, C.J.H., Blackwell, P.G., Buck, C.E., Burr, G.S., Cutler, K.B., Damon, P.E., Edwards, R.L., Fairbanks, R.G., Friedrich, M., Guilderson, T.P., Hogg, A.G., Hughen, K.A., Kromer, B., McCormac, G., Manning, S., Ramsey, C.B., Reimer, R.W., Remmele, S., Southon, J.R., Stuiver, M., Talamo, S., Taylor, F.W., van der Plicht, J., Weyhenmeyer, C.E., 2004. IntCal04 terrestrial radiocarbon age calibration, 0–26 cal kyr BP. Radiocarbon 46, 1029–1058.
Rozanski, K., Araguas-Araguas, L., Gonfiantini, R., 1993. Isotopic patterns in modern global precipitation. In: Swart, P.K., Lohmann, K.C., McKenzie, J., Savin, S. (Eds.), Climate Change in Continental Isotopic Records, vol. 78. American Geophysical Union, Washington, DC, pp. 1–36.
Schrag, D.P., Hampt, G., Murray, D.W., 1996. Pore fluid constraints on the temperature and oxygen isotopic composition of the glacial ocean. Science 272, 1930–1932.
Shakun, J.D., Carlson, A.E., 2010. A global perspective on last glacial maximum to Holocene climate change. Quaternary Science Reviews 29, 1801–1816.
Shen, C.-C., Edwards, R.L., Cheng, H., Dorale, J.A., Thomas, R.B., Moran, S.B., Weinstein, S.E., Hirschmann, M., 2002. Uranium and thorium isotopic and concentration measurements by magnetic sector inductively coupled plasma mass spectrometry. Chemical Geology 185, 165–178.
Shen, C.-C., Cheng, H., Edwards, R.L., Moran, S.B., Edmonds, H.N., Hoff, J.A., Thomas, R.B., 2003. Measurement of attogram quantities of ^{231}Pa in dissolved and particulate fractions of seawater by isotope dilution thermal ionization mass spectroscopy. Analytical Chemistry 75, 1075–1079.
Sirocko, F., Garbe-Schönberg, D., McIntyre, A., Molfino, B., 1996. Teleconnections between the subtropical monsoons and high-latitude climates during the last deglaciation. Science 272, 526–529.
Steffensen, J.P., Andersen, K.K., Bigler, M., Clausen, H.B., Dahl-Jensen, D., Fischer, H., Goto-Azuma, K., Hansson, M., Johnsen, S.J., Jouzel, J., Masson-Delmotte, V., Popp, T., Rasmussen, S.O., Röthlisberger, R., Ruth, U., Stauffer, B., Siggaard-Andersen, M.-L., Sveinbjörnsdóttir, Á.E., Svensson, A., White, J.W.C., 2008. High-resolution Greenland ice core data show abrupt climate change happens in few years. Science 321, 680–684.
Stocker, T.F., Johnsen, S.J., 2003. A minimum thermodynamic model for the bipolar seesaw. Paleoceanography 18. doi:10.1029/2003PA000920.
Stouffer, R.J., Yin, J., Gregory, J.M., Dixon, K.W., Spelman, M.J., Hurlin, W., Weaver, A.J., Eby, M., Flato, G.M., Hasumi, H., Hu, A., Jungclaus, J.H., Kamenkovich, I.V., Levermann, A., Montoya, M., Murakami, S., Nawrath, S., Oka, A., Peltier, W.R., Robitaille, D.Y., Sokolov, A., Vettoretti, G., Weber, S.L., 2006. Investigating the causes of the response of the thermohaline circulation to past and future climate changes. Journal of Climate 19, 1365–1387.
Stuiver, M., Polach, H.A., 1977. Reporting of C-14 – discussion. Radiocarbon 19, 355–363.
Svensson, A., Andersen, K.K., Bigler, M., Clausen, H.B., Dahl-Jensen, D., Davies, S.M., Johnsen, S.J., Muscheler, R., Parrenin, F., Rasmussen, S.O., Roethlisberger, R., Seierstad, I., Steffensen, J.P., Vinther, B.M., 2008. A 60,000 year Greenland stratigraphic ice core chronology. Climate of the Past 4, 47–57.
Wang, L.J., Sarnthein, M., Grootes, P.M., Erlenkeuser, H., 1999. Millennial reoccurrence of century-scale abrupt events of East Asian monsoon: a possible heat conveyor for the global deglaciation. Paleoceanography 14, 725–731.

Wang, X., Auler, A.S., Edwards, R.L., Cheng, H., Cristalli, P.S., Smart, P.L., Richards, D.A., Shen, C.-C., 2004. Wet periods in northeastern Brazil over the past 210 kyr linked to distant climate anomalies. Nature 432, 740–743.

Wang, Y.J., Cheng, H., Edwards, R.L., An, Z.S., Wu, J.Y., Shen, C.-C., Dorale, J.A., 2001. A high-resolution absolute-dated late Pleistocene monsoon record from Hulu Cave, China. Science 294, 2345–2348.

Wang, Y.J., Cheng, H., Edwards, R.L., He, Y.Q., Kong, X.G., An, Z.S., Wu, J.Y., Kelly, M.J., Dykoski, C.A., Li, X.D., 2005. The Holocene Asian monsoon: links to solar changes and North Atlantic climate. Science 308, 854–857.

Wang, Y.J., Cheng, H., Edwards, R.L., Kong, X.G., Shao, X.H., Chen, S.T., Wu, J.Y., Jiang, X.Y., Wang, X.F., An, Z.S., 2008. Millennial- and orbital-scale changes in the East Asia monsoon over the past 224000 years. Nature 451, 1090–1093.

Yang, Y., Yuan, D.X., Cheng, H., Zhang, M.L., Qin, J.M., Lin, Y.S., Zhu, X.Y., Edwards, R.L., 2010. Precise dating of abrupt shifts in the Asian monsoon during the last deglaciation based on stalagmite data from Yamen Cave, Guizhou Province, China. Science in China. Series D, Earth Sciences 53, 633–641.

Yuan, D.X., Cheng, H., Edwards, R.L., Dykoski, C.A., Kelly, M.J., Zhang, M.L., Qing, J.M., Lin, Y.S., Wang, Y.J., Wu, J.Y., Dorale, J.A., An, Z.S., Cai, Y.J., 2004. Timing, duration, and transitions of the last interglacial Asian monsoon. Science 203, 575–578.

Zhang, P., Cheng, H., Edwards, R.L., Chen, F., Wang, Y., Yang, X., Liu, J., Tan, M., Wang, X., Liu, J., An, C., Dai, Z., Zhou, J., Zhang, D., Jia, J., Jin, L., Johnson, K.R., 2008. A test of climate, sun, and culture relationships from an 1810-year Chinese cave record. Science 322, 940–942.